

Effect of Organic Matter and Thermal Maturity on Methane Adsorption Capacity on Shales from the Middle Magdalena Valley Basin in Colombia

Olga Patricia Ortiz Cancino,*,† Deneb Peredo Mancilla,‡ Manuel Pozo,§ Edgar Pérez, and David Bessieres **

ABSTRACT: High-pressure methane adsorption isotherms were measured on five shale core samples obtained during exploratory drilling from three boreholes located in the Colombian Middle Magdalena Valley Basin. The experiments were carried out at 50 and 75 °C and for pressures ranging up to 3.5 MPa under dry conditions through the use of a homemade manometric setup. The effect of the total organic carbon (TOC) content, thermal maturity, clay content, and specific surface area (SSA) on methane adsorption capacity has been discussed. The excess adsorption data were fitted to a three-parameter (n_1, p_1, \dots, p_n) and ρ_{ads}) Langmuir model with the value of the adsorbed phase density, ρ_{ads} maintained fixed at 421 kg/m³, which corresponds to liquid-phase density of methane at a normal boiling point. An excellent fit to the experimental data was achieved. The results show that the temperature has a negative effect on the adsorption capacity, while TOC has a positive effect, even if no linear regression was found between TOC and methane adsorption capacity. No correlation was observed between the clay content and the TOC-normalized adsorption capacity to methane, which indicates that clay minerals do not significantly contribute to methane adsorption in the case of our samples. In addition, there is not a general trend between TOC normalized and thermal maturity. Among the factors investigated in the present study, TOC has the major contribution to the adsorption uptake. A similar contribution is found for the SSA, which is consistent, considering the positive correlation between TOC and SSA. This set of data represents meaningful information for indirect estimations of the gas in place during the future recovery strategies. This study furthers the ongoing projects on the understanding of the adsorption effect on shale gas production and assessment.

1. INTRODUCTION

In 2016, according to the BP Statistical Review of World Energy, the natural gas production of Colombia was almost equal to its consumption and the reserves/production (R/P) ratio was close to 12. At the present time, almost all of the natural gas production of country comes from conventional reserves, which could be empty by the year 2028; meanwhile, unconventional technically recoverable gas reserves are estimated to be 12 times greater than conventional reserves. Shale gas has become an increasingly important source of natural gas supply.

It is of general acceptance that natural gas can be stored in shales in three different ways: as free gas, adsorbed gas, and dissolved gas,³⁻⁸ with adsorbed gas being the main contribution (up to 85%). 3,9-12 Therefore, the quantity of adsorbed gas represents one of the most important parameters in gas shale reserves and production estimations. 13 In this sense, many laboratory experiments have been carried out on methane adsorption in shale gas from different worldwide basins, with the objective to provide a better understanding of this phemomenon. 7,14-23 In addition to adsorption measurements, some works had obtained at the same time the stored free-gas amount, with the confining-stress effect having been taken into account.24-26

Adsorption is a complex process, which depends upon the rock matrix and fluid properties as well as reservoir conditions (e.g., temperature and pressure). The main parameters affecting adsorption capacity are the total organic carbon (TOC) content, mineralogy, water content, temperature, and pressure. Most of the studies affirm that organic matter, TOC, is the main factor that controls adsorption uptake in shales. 8,18-23 It has also been reported that the type of kerogen as well as its maturity can influence the adsorption ability in such a way that the methane adsorption capacity of kerogen decreases in the sense of type III > type II, 7,18 while a higher maturity means a higher adsorption capacity. 8,20,27 Others studies reported that sorption capacity will first increase and then decrease with maturity. 28,29

The roles of shale mineral composition and pore structure have been largely studied.^{8,28} In addition to organic matter, clay mineral may provide a contribution upon adsorption capacity. 4,7,8,23,27,30-32 Montmorillonite and illite/smectite present a higher adsorption capacity than kaolinite, chlorite, and illite. 30 At a nanometric scale, it is difficult to correlate the adsorption gas capacity

Received: June 30, 2017 Revised: September 27, 2017 Published: September 28, 2017



[†]Universidad Industrial de Santander, Bucaramanga, Santander 680002, Colombia

[‡]Université de Pau et des Pays de l'Adour, CNRS, UMR 5150, Laboratoire des Fluides Complexes et leurs Réservoirs, TOTAL, 64013 Pau, France

[§]Department of Geology and Geochemistry, Universidad Autónoma de Madrid (UAM), Cantoblanco, 28049 Madrid, Spain

Instituto Colombiano del Petróleo (ICP), Piedecuesta, Santander 681018, Colombia

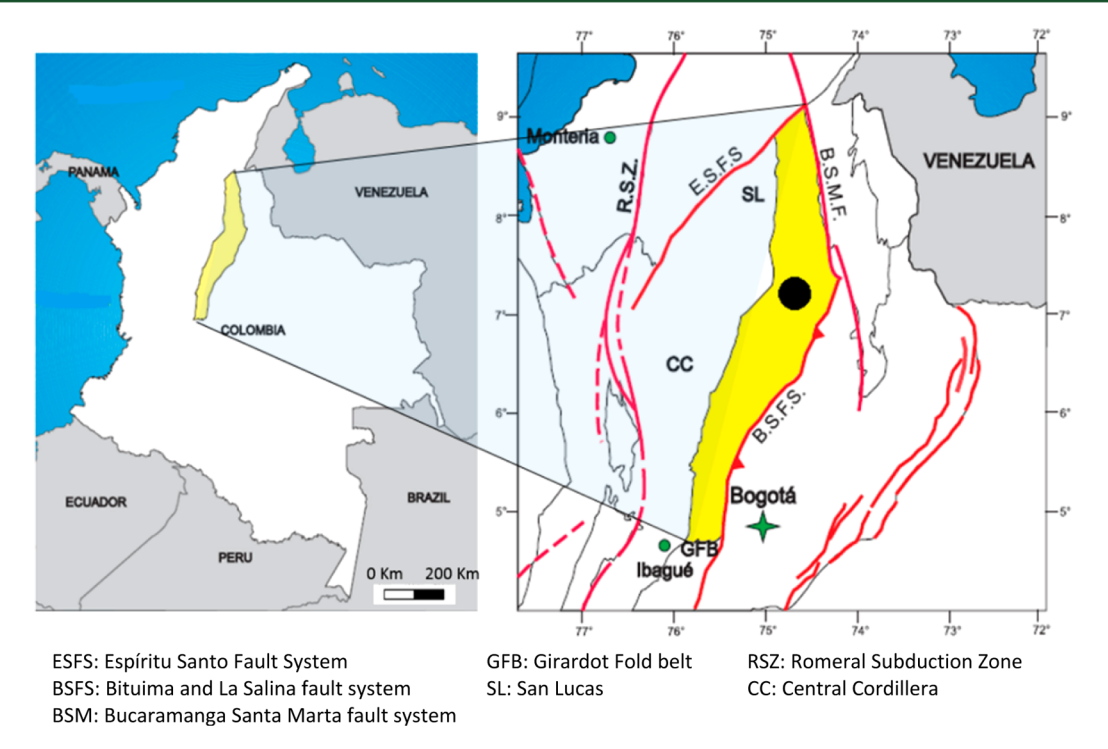


Figure 1. Location of the Middle Magdalena Valley (in yellow) and sample site (black circle) [modified with permission from ref 40. Copyright 2007 Agencia Nacional de Hidrocarburos (ANH)].

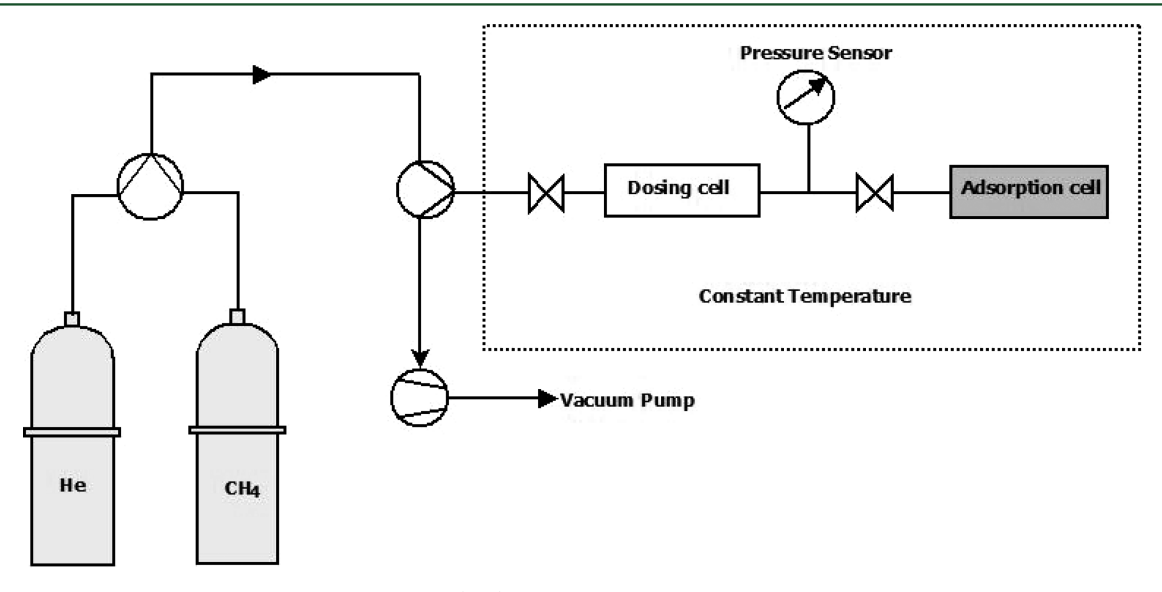


Figure 2. Schematic diagram of the HP/high-temperature (HT) manometric setup.

directly with the total organic content as a result of the pore size distribution and heterogeneity of the surface; therefore, some authors suggest that the adsorbed gas volume evaluation should also be related to the surface area. The adsorption in clay-rich shales is due to their high internal area. Therefore, the specific surface area (SSA) plays a significant role in gas adsorption as a result of the microporosity associated with organic matter. Zhang et al. Teport that shales with a higher content of clay minerals and a similar TOC content have a larger SSA. This is due to the porosity hosted in the clay minerals.

Pressure increases the adsorption capacity to some extent when it rises isothermally.³⁸ In contrast, the water content and temperature have a negative influence. Water may occupy the adsorption sites, hence reducing the amount of adsorbed gas.^{20,39}

A reduction in gas adsorption up to 40% has been found when comparing moisture samples to dry samples.^{7,8} The temperature is also one of the factors influencing the state of shale gas. With gas adsorption being an exothermic process, the adsorption capacity of shale decreases with an increasing temperature.^{6,2,3} The combined effect of the pressure and temperature can be used during the production stage because it represents gas desorption behavior.¹¹ Although the above-mentioned parameters are the most studied, some works have been performed focused to dynamically changing pore volume adjustments as a result of the adsorption layer taking up space and overburden effects on core shale samples.^{24–26}

This review highlights that gas storage in shale is a complex multi-parameter process. An understanding and quantification

Table 1. Depth and Miner	alogical Analysi	is of the Samples
--------------------------	------------------	-------------------

sample	depth (m)	illite (%, w/w)	kaolinite (%, w/w)	quartz (%, w/w)	calcite (%, w/w)	pyrite (%, w/w)	gypsum (%, w/w)	apatite (%, w/w)
S1A	2835	15	45	27	3	10	id	0
S1B	2850	11	19	54	10	6	id	0
S2A	2934	9	21	31	33	4	id	<2
S2B	3004	13	15	11	50	9	id	<2
S3	4430	7	22	32	28	8	id	<2

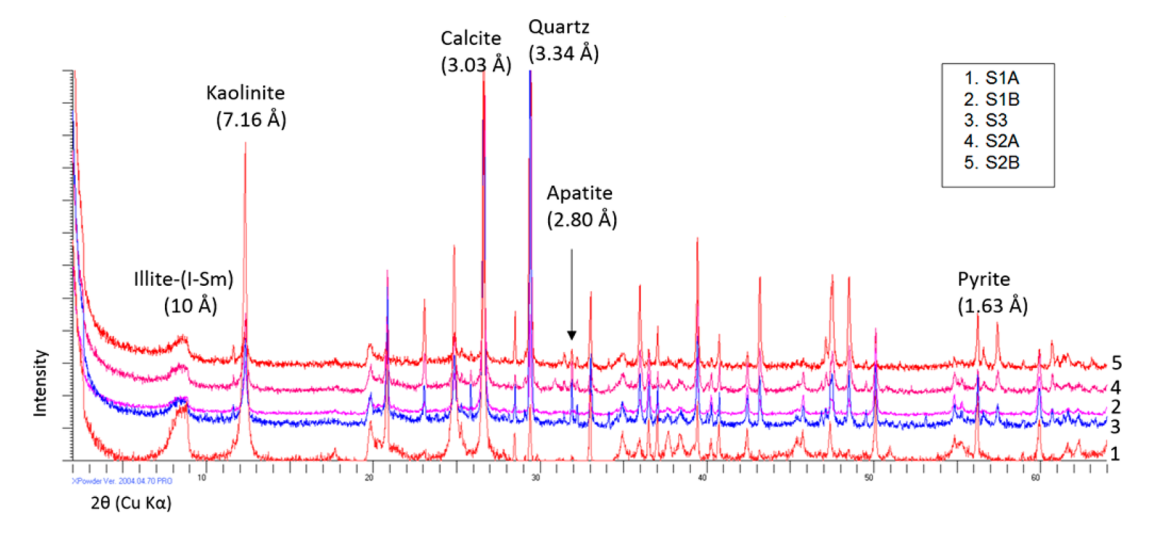


Figure 3. XRD diffractograms of bulk samples. Mineralogical assemblages include phyllosilicates (kaolinite and illite, in illite/smectite mixed layers), calcite, quartz, apatite, and pyrite. S1A shows the highest percentage of phyllosilicates (60%, mostly kaolinite), whereas the quartz content can reach 54% in S1B and the calcite content can reach 50% in S2B (see Table 1).

of each parameter require a very huge set of well-defined experimental data. Despite the growing interest, research published on shale is mostly limited to U.S. and Canadian shales, China shales, and more recently European black shales. Less studies have been reported for South American shales.

The objective of the present study is to further the set of available data. Here, we report methane adsorption data for selected Colombian shales from the Middle Magdalena Valley. Using a homemade manometric setup, methane adsorption isotherms were reported at 50 and 75 $^{\circ}\mathrm{C}$ for pressures up to 3.5 MPa. These measurements were carried out on dried samples from cores belonging to three different wells.

Following recommendations of previous works devoted to shales, the methodology applied in this work is as follows: (1) geochemical and textural characterization of the samples, (2) CH₄ adsorption capacity over ranges of pressure and temperature, with representation of the adsorption data by a modified Langmuir approach, and (3) variation of the CH₄ uptake as a function of the Brunauer–Emmett–Teller (BET) surface area, organic matter richness, clay content, and thermal maturity.

This comprehensive work furthers the still limited reliable database of adsorption data on shales. To the best of our knowledge, this is the first study devoted to Colombian gas shales.

2. MATERIALS AND EXPERIMENTAL METHODOLOGY

2.1. Materials. Five core samples were obtained during exploratory drilling (stratigraphic wells) of three boreholes located in the Middle Magdalena Valley Basin in Colombia. As a result of confidentiality reasons, detailed locations are not disclosed, and the samples are named S1A, S1B, S2A, S2B, and S3.

The Middle Magdalena Valley Basin is 34 000 km². It is stretched along the middle reaches of the Magdalena river and is bound to the north and south by the Espiritu Santo fault system (ESFS) and the

Girardot fold belt (GFB), respectively. To the northeast, the basin is limited by the Bucaramanga—Santa Marta fault system (BSMF), and to the southeast, the basin is limited by the Bituima and La Salina fault system (BSFS). The western limit is marked by the westernmost onlap of the Neogene basin fill into the Serranía de San Lucas (SL) and the Central Cordillera (CC) basement, ⁴⁰ as shown in Figure 1. The black circle shows the location of the wells in the proximity of Barrancabermeja.

2.2. Sample Characterization. 2.2.1. X-ray Diffraction (XRD) Analysis. Mineralogical analysis of samples was carried out by means of XRD using Siemens D-5000 equipment with a scanning speed of 1° (2θ)/min and Cu K α radiation (40 kV and 20 mA). XRD is the most widely used technique for identification of minerals. When an incident beam of X-ray interacts with crystalline matter (regular structure), the diffraction (constructive interference) can occur for certain directions, giving a set of reflections characteristic of the analyzed substance (fingerprint). The diffraction reflections are related to spacing of atomic planes in a sample (i.e., d spacing) and wavelength of X-rays (λ).

XRD studies were achieved on both randomly oriented samples (bulk sample) and clay fraction samples ($<2 \mu m$). Powdered whole-rock

Table 2. Rock-Eval Analysis, HI, OI, and SSA (BET Method)^a

sample	T_{\max} (°C)	TOC (%)	S1	S2	S3	HI	OI	SSA
S1A	459	3.8	1.93	3.75	0.14	99	3.69	6.9
S1B	463	4.7	2.00	3.61	0.23	78	4.94	10.28
S2A	478	3.1	0.35	0.70	0.18	22	5.76	13.05
S2B	487	8.8	0.39	1.90	0.42	22	4.79	26.29
S3	471	5.7	2.47	4.96	0.25	87	4.37	10.59

 $^{\prime\prime}T_{max\prime}$ thermal maturation parameter; TOC, total organic carbon (wt %); S1, free HC (mg of HC/g of rock); S2, oil potential (mg of HC/g of rock); S3, CO₂ organic source (mg of CO₂/g of rock); HI, hydrogen index; OI, oxygen index; and SSA, specific surface area (m²/g of rock).

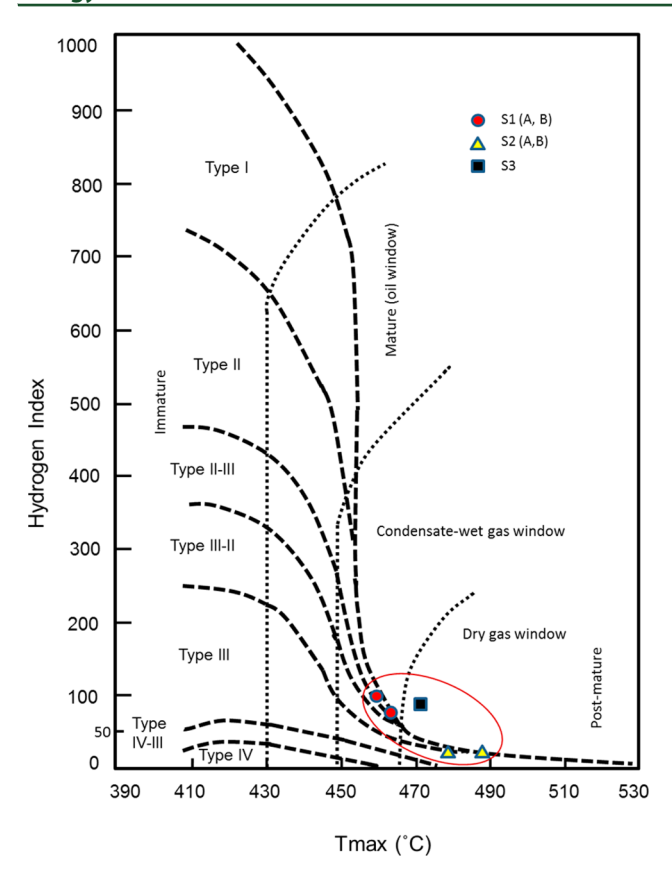


Figure 4. T_{max} -HI plot.

samples (milled and dry sieved at <63 μ m for homogenization) were scanned from 2° to 65° (2 θ). The method of the mineral intensity factors (MIFs) was applied to XRD peak intensity ratios normalized to 100% with calibration constants for the quantitative estimation of the mineral contents. ⁴¹ The clay fraction (<2 μ m) was separated by centrifugation, and samples were prepared from suspensions oriented on glass slides. Identification of the clay fraction minerals was performed on oriented air-dried samples and solvated with ethylene glycol after heating at 550 °C.

2.2.2. SSA. The SSA of minerals is one of their most important properties controlling surface phenomena. The most widely used technique for determining SSA is based on gas adsorption, notably of

nitrogen gas. Adsorption isotherms, describing the amount of gas adsorbed as a function of the relative pressure (p/p_0) , can exhibit different features depending upon the size of particles, the presence of organized pores, and the energetic properties of the mineral surface. Different methods of data analysis are used to derive quantitative information from experimental adsorption curves, of which BET⁴² analysis is the most common. The BET SSA of powdered samples was analyzed by Micromeritics ASAP 2010 equipment and determined from a low-pressure nitrogen adsorption isotherm at 77 K (-196 °C).

2.2.3. Rock-Eval Analysis. The Rock-Eval analysis of the selected whole rock samples was performed by a Rock-Eval VI pyrolyser. The interesting parameters measured include TOC, $T_{\rm max}$ S1 [free hydrocarbons (HC)], S2 (oil potential), S3 (CO₂ organic source and carbonate), and related indices: oxygen index (OI) and hydrogen index (HI).

2.3. Methane Adsorption Measurements. *2.3.1. Sample Preparation.* Considering that the time required to reach the equilibrium on intact core samples could be extremely long as a result of the low permeability of shales, ⁴³ the samples were split. However, dependent upon the organic matter distribution, the milling process may induce variations on the available surface. Following the recommendations of Gasparik et al., ²⁰ cuttings of different particles sizes were tested. ⁵ For each sample, two particle size fractions ranging from 1 to 1.5 mm and from 1.5 to 5 mm were investigated. A known mass of each sample was introduced into the adsorption cell (Figure 2) and dried at 105 °C for 24 h to remove the moisture. The mass was carefully measured and chosen to obtain a large enough available adsorption area; about 30 m² is the minimum area required.

2.3.2. Manometric Adsorption Setup. The instrument used in the present study is a high-pressure (HP) manometric device. A schematic view of this "homemade" apparatus is provided in Figure 2. This experimental setup and the measurement principle have been previously described.44 The main elements are the reference or dosing cell (33.57 cm³), the adsorption cell (16.56 cm³), in which the adsorbent is placed, and the pressure transducer (MKS Baratron type 121 A, with an uncertainty of 0.01% in the full scale ranging from the vacuum to 3.5 MPa). The various parts are isolated with spherical valves, thus limiting the "dead space" volume. The whole apparatus is regulated under isothermal conditions through the use of a heater wire controlled by a proportional-integral-derivative (PID) regulator (Eurotherm 3208). Five thermocouples (type K, accuracy of ± 0.1 K) were placed in different parts of the circuit to check that the isothermal conditions are applied along the circuit during the measurement. The overall uncertainty of the amount adsorbed (as a result of the helium calibration procedure and pressure accuracy) is determined to be lower than 1% over the entire (p and T) range investigated in this study.

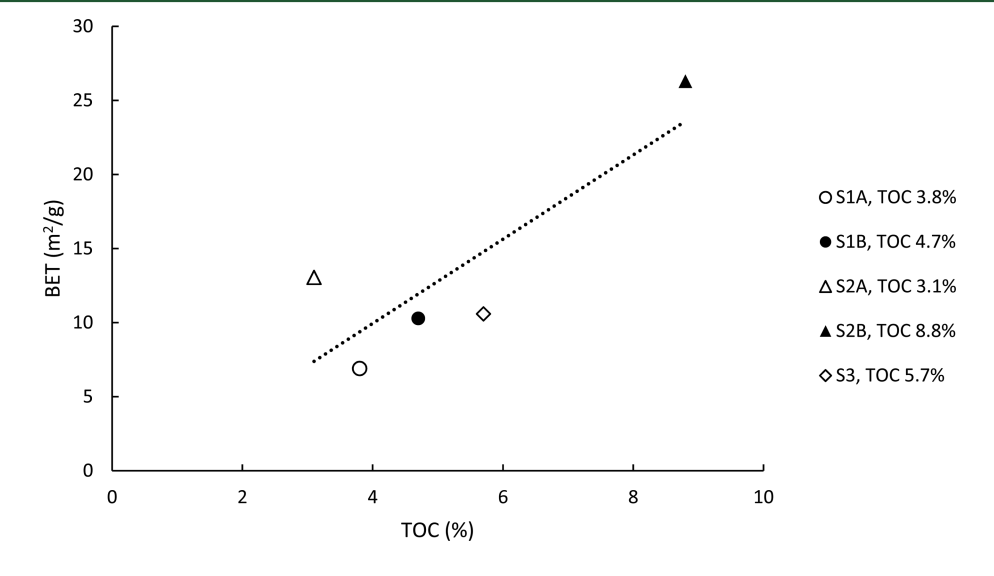


Figure 5. Correlation between BET and TOC. Note a moderate linear correlation.

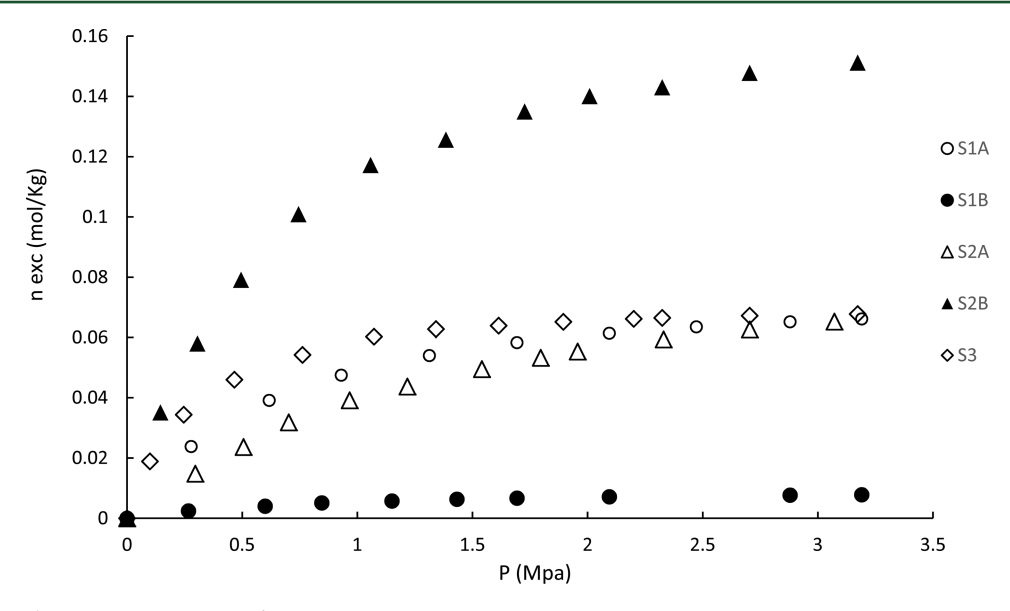


Figure 6. Methane adsorption capacity at 50 °C.

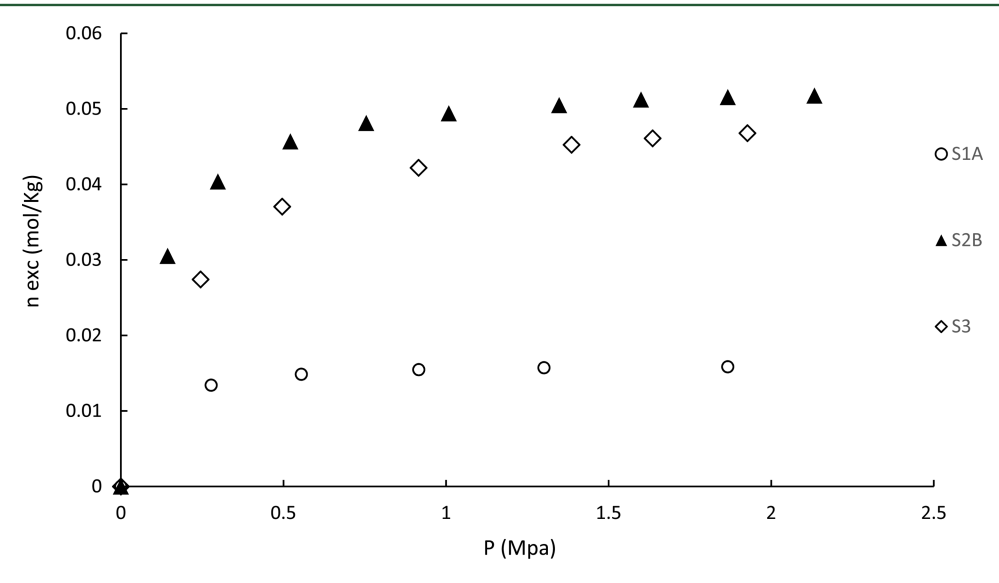


Figure 7. Methane adsorption capacity at 75 °C.

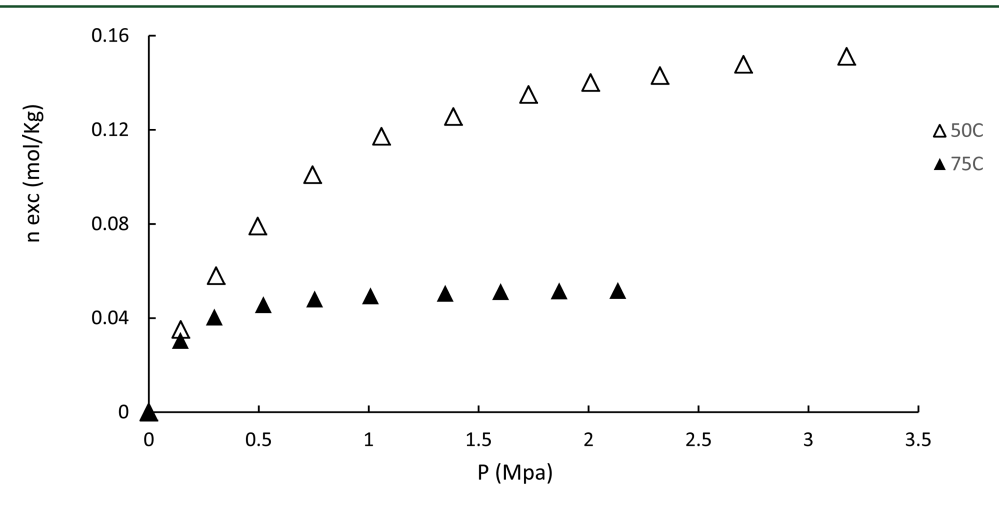


Figure 8. CH₄ adsorption capacity for sample S2B at 50 and 75 °C.

2.3.3. Calculation of Excess Adsorption. The adsorption isotherms were determined using an accumulative process, with a value of

increased pressure about 2–3 bar between successive gas doses. The procedure consists of expanding a gas from the dosing volume $V_{\rm D}$

Table 3. Langmuir Model Fitting Parameters at 50 °C

sample	$n_{\rm L} \; ({\rm mol/kg})$	$p_{\rm L}~({ m MPa})$	Δn
S1A	0.0848	0.711	0.00098
S2A	0.1054	1.661	0.00017
S2B	0.1926	0.680	0.00040
S3	0.0783	0.315	0.00001

Table 4. Langmuir Model Fitting Parameters at 75 °C

sample	$n_{\rm L}~({ m mol/kg})$	$p_{\rm L}~({ m MPa})$	Δn
S1A	0.0169	0.071	0.00002
S2B	0.0562	0.118	0.00010
S3	0.0537	0.229	0.00021

(dosing cell) into the adsorption cell $(V_{\rm M})$, which contains the sample under isothermal conditions. Application of this experimental methodology requires the previous determination of the two volumes $V_{\rm D}$ and $V_{\rm M}$. The uncertainty of these measures is inferior to 0.5% in both cases. The mass balance involves the void volume or volume accessible in the presence of the adsorbent, which is a key parameter for the adsorption capacity. The void volume was determined through helium expansions at each temperature and for different pressures. The choice of helium was dictated considering it is an inert, non-sorbing gas. An additional drying is performed after that for 8–10 h. The methane molar volume considered at the experimental conditions (p and T) is determined with the Span and Wagner equation of state (EOS). The return to the thermodynamic equilibrium was controlled by the pressure value. It should be observed that it was reached in a range from 45 to 60 min.

2.3.4. Parameterization of Excess Adsorption Isotherms. Because reservoir pressures are higher than the experimental pressures, it is necessary to extrapolate data to well pressure conditions. Therefore, the experimental data were parametrized using a fitting procedure. Several approaches have been developed^{4,46–48} to this purpose. The modified Langmuir model is used as a standard model to describe vapor isotherms on shales,⁴⁸ and it is widely accepted in the petroleum industry.³³ This model includes the adsorbed gas density as a fitting parameter. Because this value is difficult to assess, most of the studies have shown a good match when assuming it as the methane liquid density at a normal boiling point.^{4,12,39,49,50}

The experimental data were correlated using a three-parameter Langmuir model described by Gensterblum et al. 51 and applied by Gasparik et al. 4

$$n_{\mathrm{ads}}^{\mathrm{excess}} = n_{\mathrm{L}} \frac{p}{p + p_{\mathrm{L}}} \left(1 - \frac{\rho_{\mathrm{g}}(p, T)}{\rho_{\mathrm{ads}}} \right) = n_{\mathrm{ads}}^{\mathrm{absolute}} \left(1 - \frac{\rho_{\mathrm{g}}(p, T)}{\rho_{\mathrm{ads}}} \right)$$

in which $n_{\rm ads}^{\rm excess}$ is the adsorbed amount of gas (mol/kg) at p (MPa), $p_{\rm L}$ is the Langmuir pressure, corresponding to the pressure at which half of the adsorption sites are occupied (monolayer), $n_{\rm L}$ is the amount adsorbed (mol/kg) when all of the monolayer is filled (maximum Langmuir capacity), $\rho_{\rm g}$ is the gas density (kg/m³) at p and T, and $\rho_{\rm ads}$ (kg/m³) is the adsorbed phase density, which was assumed as a fixed value of 421 kg/m³ for the adsorbed phase density. 12,19,52

Standard deviation was calculated according to⁵

$$\Delta n = \frac{1}{N} \sqrt{\sum_{1}^{N} (n_{\rm exp} - n_{\rm fit})^2}$$

where N is the number of experimental data points and $n_{\rm exp}$ and $n_{\rm fit}$ are experimental measured data and fitted data, respectively. The results are shown in the next section.

3. RESULTS

3.1. Mineralogy. The XRD mineralogical analysis revealed that the five bulk-rock samples are mostly made up of phyllosilicates (28-60%), quartz (11-54%), and calcite (3-50%). Other minerals include pyrite (4-10%), apatite (<2%), and traces of gypsum (see Table 1). The sample S1A shows the highest content in phyllosilicates (>50%) and pyrite. The remaining samples have a phyllosilicate content up to 30%, whereas quartz can reach 54% in S1B and calcite can reach 50% in S2B. The value of d(060) reflection is in all cases 1.49–1.50 Å, indicating dioctahedral phyllosilicates. The oriented aggregates of the clay fraction ($<2 \mu m$) show that samples are mostly composed of two clay minerals: kaolinite and illite. In the bulk sample, the kaolinite content is ranging between 15% (S2B) and 45% (S1A). Illite is subordinated (7-15% in the bulk sample) and always include traces of illite/smectite mixed layers. Two representative XRD patterns of bulk samples are shown in Figure 3.

3.2. Organic Matter Richness and Thermal Maturity. Rock-Eval analysis can help to know the oil—gas potential of a rock but also the type of organic matter and degree of maturation. The most interesting parameters measured are shown in Table 2.

TOC is ranging between 3.12% (S2A) and 8.77% (S2B). TOC is the amount of organic carbon present in the sample. In shales, TOC of 2–5% is considered good and higher than 5% very good. ⁵³ All analyzed samples have TOC higher than 3% and, in the case of S3 and S2B, higher than 5%.

Besides, TOC is important to consider the level of thermal maturation, which can be given by the $T_{\rm max}$ value. This parameter

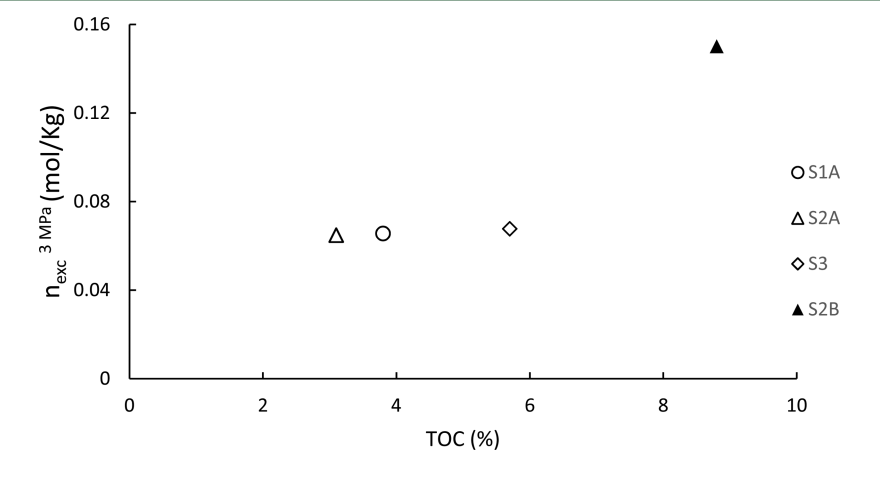


Figure 9. CH₄ adsorption capacity n_{excess} (at 3 MPa and 50 °C) as a function of TOC.

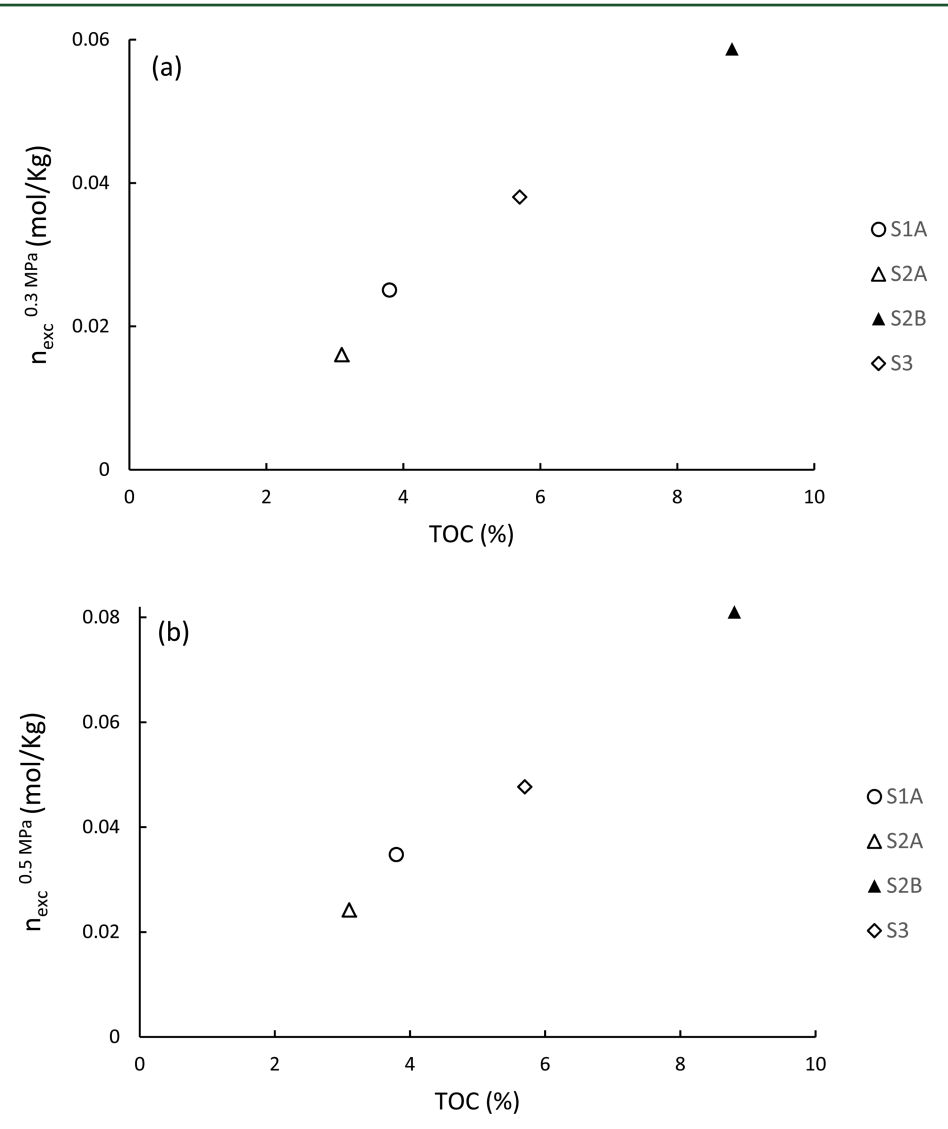


Figure 10. CH₄ adsorption capacity at 50 °C as a function of TOC at (a) 0.3 MPa and (b) 0.5 MPa.

is the temperature at which the maximum amount of HC degraded from kerogen was generated. The $T_{\rm max}$ values range between 459 and 487 °C (Table 2). In general, according to Peters, 55 T_{max} values lower than 435 °C are considered immature organic matter but T_{max} values between 435 and 455 °C indicate "oil window" conditions (mature organic matter). Higher values of $T_{\rm max}$ between 455 and 470 °C are considered transitional, and higher values than 470 °C represent the wet gas zone (overmature organic matter). Indeed, when more mature is the rock, the higher is the temperature (T_{max}) required to release HC from kerogen. Sample S1A shows a lower $T_{
m max}$ value (459 °C); samples S1B, S2A, and S3 show intermediate values (463-478 °C); and sample S2B shows the highest value (487 °C). Therefore, the maturation order is S2B > S2A > S3 >S1B > S1A. According to the T_{max} -HI plot, all of the samples are within the post-mature stage but samples S1A and S1B are within the condensate-wet gas zone, whereas samples S2A and S2B are within the dry gas window conditions and sample S3 is between them (Figure 4). The samples S3, S2A, and especially S2B $(T_{\text{max}} > 470 \text{ }^{\circ}\text{C})$ are indicative of overmature organic

With regard to S1 (free HC) and S2 (oil potential), the concentrations are low and range between 0.35 mg of HC/g of

rock (sample S2A) and 2.47 mg of HC/g of rock (sample S3) for parameter S1 and between 0.7 mg of HC/g of rock (sample S2A) and 4.96 mg of HC/g of rock (sample S3) for parameter S2. The relative amounts of parameters S1 and S2 depend upon the type of organic matter but also the duration and temperature suffered by the rock. Parameter S3 indicates CO_2 evolved from thermal cracking during pyrolysis, reaching the highest value in sample S2B (0.42 mg of CO_2/g) and the lowest value in sample S1A (0.14 mg of CO_2/g).

The OI is derived from the ratio (S3/TOC) \times 100, ranging from 3.69 (sample S1A) to 5.76 (sample S2A). The HI is derived from the ratio (S2/TOC) \times 100, reaching 22 in samples S2A and S2B, between 78 and 87 in samples S1B and S3, and the highest value in sample S1A (99). The type of kerogen present in a rock determines its quality. Type I kerogen is the highest quality, and type III is the lowest. The values of T_{max} HI, and OI in the studied samples let us to include them as kerogen of types II—III (samples S1A, S1B, and S3) to type II (samples S2A and S2B), according to classifications by Peters, So Gorin and Feist-Burkhardt, and Xu and co-workers (Figure 4). The maturation degree can affect the determination of the kerogene type. Indeed, the T_{max} -HI and HI–OI plots are especially useful to determine kerogen type of immature rocks.

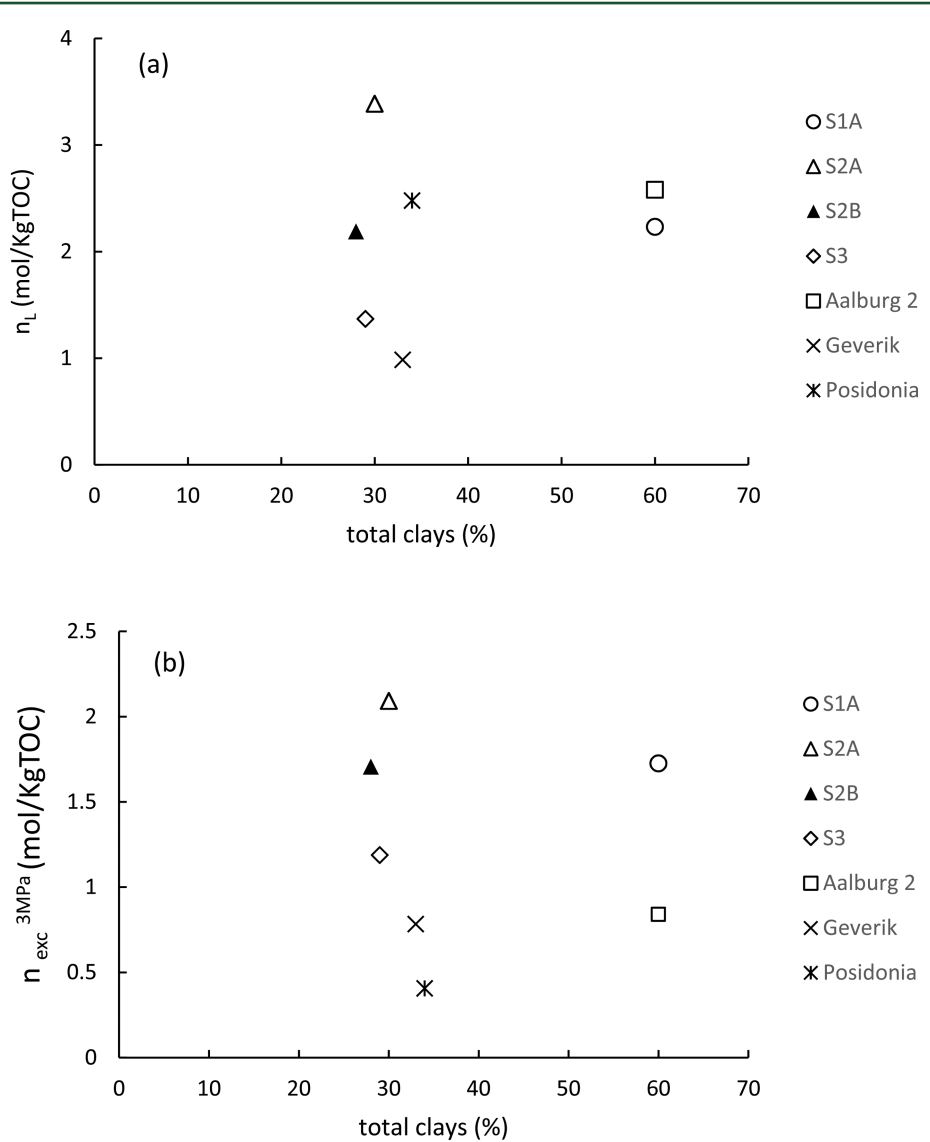


Figure 11. (a) TOC-normalized Langmuir adsorption capacity (n_L) content and (b) TOC-normalized adsorption capacity at 3 MPa as a function of the total clay content, in our work and literature data.

However, when a source rock is under maturation, the amount of hydrogen and oxygen relative to carbon decreases and then the ratios tend to converge toward the origin of the plot. Therefore, in post-mature rocks, HI and OI are not actually indicative of the original kerogen quality.

3.3. SSA. The BET SSA is ranging between 6.90 and $26.29 \text{ m}^2/\text{g}$, with the highest value in sample S2B (Table 2). Several authors reported a relationship between kerogen characteristics (thermal maturity, composition, and type) and development of nanopores enhancing the gas adsorption capacity of shales. $^{18,33,58-60}$ This fact explains the higher BET values obtained in more mature samples S2A and S2B ($13.05-26.29 \text{ m}^2/\text{g}$) when compared to the other samples ($6.9-10.59 \text{ m}^2/\text{g}$). The development of nanopores in kerogen can lead to an increase in adsorption sites with increasing TOC for the mature to postmature shales. Moreover, the analyzed samples show moderate positive correlation between TOC and BET SSA values ($R^2 = 0.71$) because of increasing adsorption sites with maturation and TOC content (Figure 5).

3.4. Methane Adsorption Isotherms (Dry Samples). CH_4 adsorption isotherms were measured at 50 °C for all of the

samples up to 3.5 MPa and for some of them (samples S1A, S2B, and S3) at 75 °C (up to pressures of 2 MPa). To obtain reliable adsorption data at a high pressure is quite complicated.⁵⁹ As a result of the limitations of our own techniques, very reliable data are accessible up to moderate pressures. In the present work, measurements were performed with high accuracy up to a quite restricted pressure range (up to 3.5 MPa). Then, a phenomenological model applied to these data allows us to extend the pressure range and to assess the CH₄ uptake. Considering the difficulty associated with the very low adsorption in shales, a set of three measurements was performed for each isotherm. The reproducibility was always superior to 99% [average absolute deviation (AAD) inferior to 1%]. The experimental data are displayed in Figure 6 (50 °C) and Figure 7 (75 °C). Note that the sample S1B has very low adsorption capacity in comparison to the other samples or literature data.^{4–6} Alteration of this sample by oxidation may be the cause of this degradation. In this context, this sample will not be considered in the study. Figure 8 reports the effect of the temperature for sample S2B. Because the saturation of the sample was observed at 75 °C, the pressure range was limited to pressures around 2 MPa.

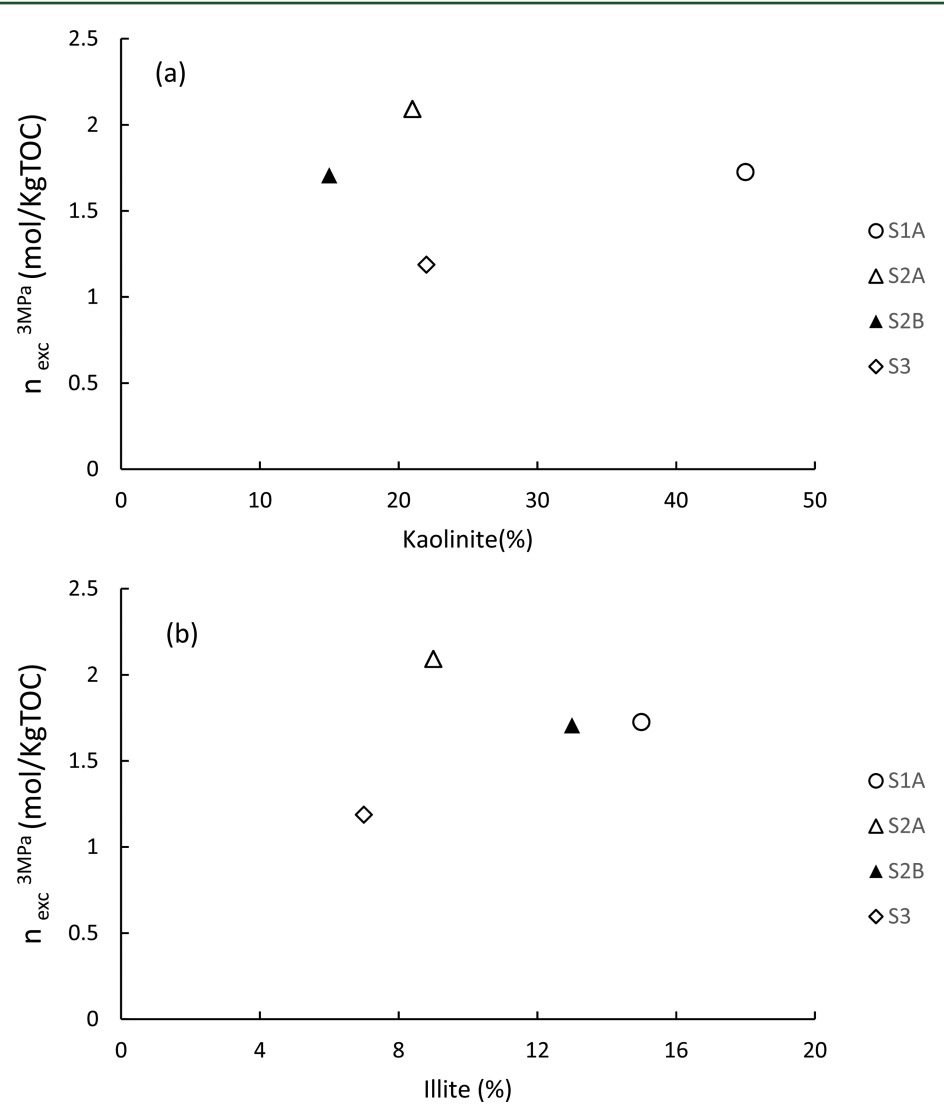


Figure 12. TOC-normalized adsorption capacity at 3 MPa as a function of the (a) kaolinite content (%) and (b) illite content (%).

Fitting parameters are shown in Tables 3 and 4, with the values of Δn in all of the samples indicating that the fitting procedure was successful and that the Langmuir model represents the adsorption behavior in a good way without restrictions. The values obtained for $n_{\rm L}$ are similar to those already reported in the literature for shales or black shales.^{4,59} In addition, such a parameter should be regarded as useful information for future assessment and exploitation of the shale wells.⁶¹ Additionally, their knowledge represents meaningful information to study the effect of individual contributions to the methane adsorption.

4. DISCUSSION

4.1. Effect of Organic Matter and Clay Contents on CH₄ Uptake. CH₄ adsorption capacity ($n_{\rm excess}$) shows a moderate positive correlation with TOC, taking into account that TOC contents of samples S1A and S2A are nearly similar (3.8 and 3.1). Even if no linear relationship can be fitted to the adsorption data, TOC remains as controlling factor of the adsorption uptake. A small discrepancy is observed for sample S3. This is shown in Figure 9, where we plot the excess adsorption capacity ($n_{\rm excess}$) at 3 MPa (and 50 °C) versus TOC.

When the adsorption uptake is plotted at a lower pressure (see panels a and b of Figure 10 at 0.3 and 0.5 MPa, respectively),

a linear law is observed between TOC and adsorption. This is due to the filling of micropores of the organic matter that occurs at a first stage during the adsorption process.

Once that the influence of TOC over the adsorption capacity was determined, the effect of the clay content was studied. One way to do this is by comparing the results with shale samples to isolated kerogen, not accessible in our case. Therefore, we follow the methodology proposed by Gasparik et al.⁴ TOC-normalized adsorption capacities were plotted versus the total clay content for all of the samples (panels a and b of Figure 11). Form the obtained figure, discrepancy of the adsorption capacities of the three samples with analogous clay contents are depicted. Meanwhile, sample S1A with a higher clay content shows adsorption capacity similar to the other samples. This lack of correlation between the clay content and the adsorption capacities is also observed with the literature data⁴ (panels a and b of Figure 11).

Similar results were observed for the detailed analysis of the individual clays plotted in panels a and b of Figure 12, the effect of illite and kaolinite seems to be insignificant in agreement with previous studies. Furthermore, while the same studies report that an important content of smectite can affect the adsorption capacity, the studied samples on the present work only presented trace amounts of illite/smectite.

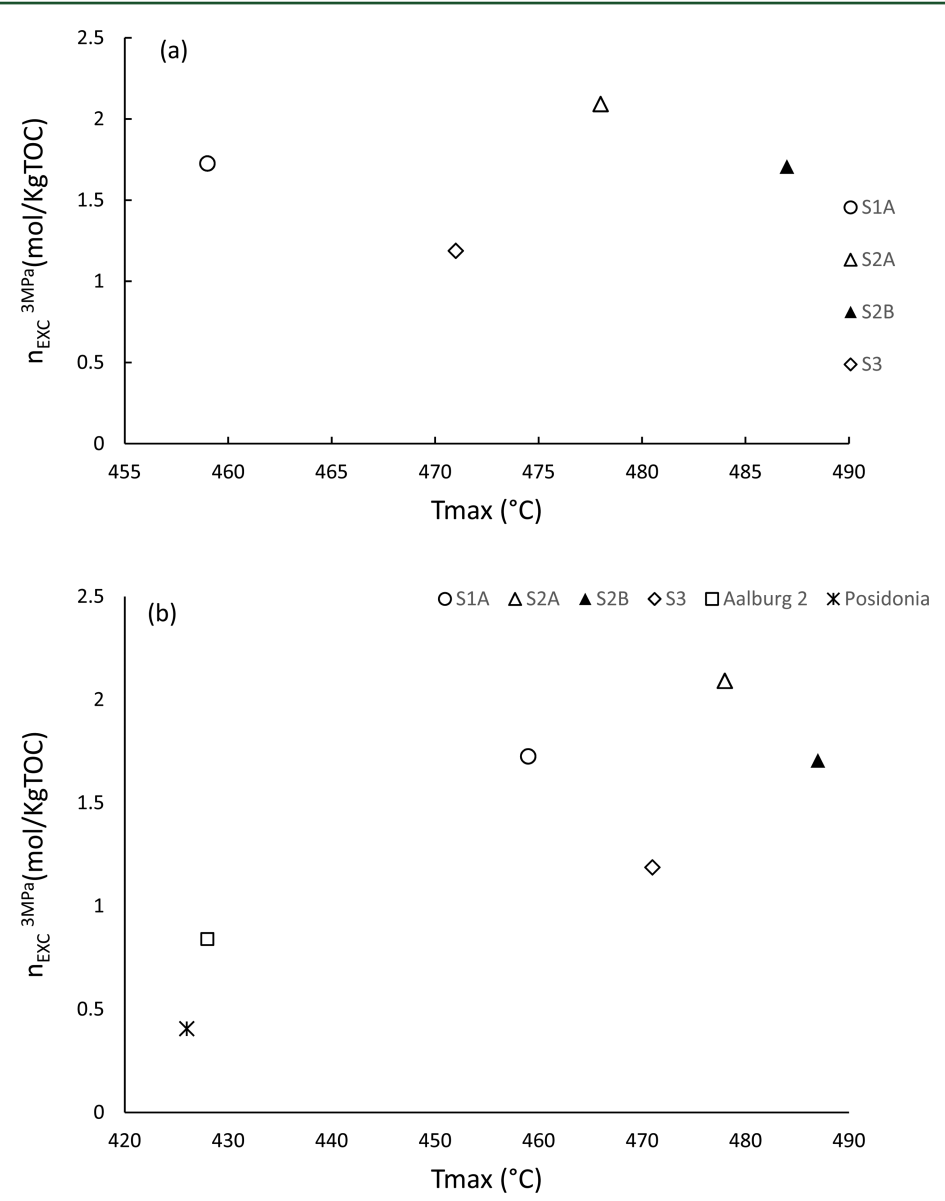


Figure 13. (a) TOC-normalized sorption capacity at 3 MPa in our work and (b) TOC-normalized adsorption capacity at 3 MPa in our work and literature data⁴ as a function of T_{max} (maturity).

4.2. Effect of Thermal Maturity. The effect of thermal maturity on the TOC-normalized excess adsorption capacity at 3 MPa $(n_{\text{excess}}^{3 \text{ MPa}})$ is shown in Figure 13a. With limitation to the samples of the present study, maturity showed no significant effect on the total amount of methane adsorbed.

Taking into account the still relatively small database, a general trend that correlates thermal maturity and adsorption capacity is not observed. A wider range of sample maturities is needed to conclude its effect over the adsorption capacity. Using data from the literature, the plot between maturity and adsorption capacity was obtained (see Figure 13b). A consistency is observed between the two sets of data. The TOC-normalized adsorption capacity linearly increases with maturity within the investigated range.

In the literature, a variety of behaviors is reported between the maturity and adsorption capacity. When the TOC-normalized adsorption capacities correlated positively with maturity in terms of vitrinite reflectance ($VR_{\rm r}$), the maximal value of $VR_{\rm r}$ was $\sim 2.5\%$, ^{4,5} which is in agreement with our observation.

5. CONCLUSION

New and reliable experimental data for methane adsorption capacities were obtained for fully characterized Colombian shales. To the best of our knowledge, this is the first study devoted to Middle Magdalena Valley shale gas. For this work, a Langmuir three-parameter model proved adequate to represent the experimental excess adsorption, allowing for the gas-in-place estimations to be obtained. The study samples showed a moderate positive relationship between TOC and SSA. The results confirmed that, even if no linear correlation was found, TOC remains a key factor defining the adsorption capacity of shales. Further work is needed to determine the importance and effect of other parameters, such as the maturity of the samples.

AUTHOR INFORMATION

Corresponding Author

*E-mail: oportizc@uis.edu.co.

ORCID

Olga Patricia Ortiz Cancino: 0000-0002-7949-348X

David Bessieres: 0000-0002-6262-4893

Notes

The authors declare no competing financial interest.

ACKNOWLEDGMENTS

The scientific work is included within the research activities of the Research Group C-144 (Geomaterials and Geological Processes, UAM). The authors are so grateful to the Colombian Petroleum Institute (ICP) for supplying the samples and letting us publishing these results. Olga Patricia Ortiz Cancino is grateful to the Universidad Industrial de Santander for the opportunity to do her Ph.D. studies at UPPA and to Colfuturo, the Embassy of France, the Colombian Ministry of National Education, and the Association of Colombian Universities (ASCUN) for financial support.

■ REFERENCES

- (1) BP. BP Statistical Review of World Energy; BP: London, U.K., June 2016.
- (2) U.S. Energy Information Administration (EIA). Technically Recoverable Shale Oil and Shale Gas Resources: An Assessment of 137 Shale Formations in 41 Countries Outside the United States; EIA: Washington, D.C., 2013.
- (3) Curtis, J. B. Fractured shale-gas systems. AAPG Bull. 2002, 86, 1921–1938.
- (4) Gasparik, M.; Ghanizadeh, A.; Bertier, P.; Gensterblum, Y.; Bouw, S.; Krooss, B. M. High-pressure methane sorption isotherms of black shales from the Netherlands. *Energy Fuels* **2012**, *26*, 4995–5004.
- (5) Gasparik, M.; Bertier, P.; Gensterblum, Y.; Ghanizadeh, A.; Krooss, B. M.; Littke, R. Geological controls on the methane storage capacity in organic-rich shales. *Int. J. Coal Geol.* **2014**, *123*, 34–51.
- (6) Guo, S. Experimental study on isothermal adsorption of methane gas on three shale samples from Upper Paleozoic strata of the Ordos Basin. *J. Pet. Sci. Eng.* **2013**, *110*, 132–138.
- (7) Ross, D. J. K.; Bustin, R. M. Characterizing the shale gas resource potential of Devonian Mississippian strata in the Western Canada sedimentary basin: Application of an integrated formation evaluation. *AAPG Bull.* **2008**, *92*, 87–125.
- (8) Ross, D. J. K.; Bustin, R. M. The importance of shale composition and pore structure upon gas storage potential of shale gas reservoirs. *Mar. Pet. Geol.* **2009**, *26*, 916–927.
- (9) Liu, G. H.; Huang, Z. L.; Jiang, Z.; Chen, J.; Chen, F.; Xing, J. Gas adsorption capacity calculation limitation due to methane adsorption in low thermal maturity shale: A case study from the Yanchang Formation, Ordos Basin. *J. Nat. Gas Sci. Eng.* **2016**, *30*, 106–118.
- (10) Montgomery, S. L.; Jarvie, D. M.; Bowker, K. A.; Pollastro, R. M. Mississippian Barnet Shale, Fort Worth basin, north-central Texas: Gas-shale play with multi-trillion cubic foot potential. *AAPG Bull.* **2005**, *89*, 155–175.
- (11) Wu, Y.; Fan, T.; Jiang, S.; Yang, X.; Ding, H.; Meng, M.; Wei, D. Methane adsorption capacities of the Lower Paleozoic Marine Shales in the Yangtze Platform, South China. *Energy Fuels* **2015**, *29* (7), 4160–4167.
- (12) Yang, F.; Ning, Z. F.; Zhang, R.; Zhao, H.; Krooss, B. M. Investigations on the methane sorption capacity of marine shales from Sichuan Basin, China. *Int. J. Coal Geol.* **2015**, *146*, 104–117.
- (13) Pan, Z.; Connell, L. D. Reservoir Simulation of free and adsorbed gas production from shale. *J. Nat. Gas Sci. Eng.* **2015**, 22, 359–370.
- (14) Hu, H. Methane adsorption comparison of different thermal maturity kerogens in shale gas system. *Chin. J. Geochem.* **2014**, 33 (4), 425–430.
- (15) Ross, D. J. K.; Bustin, R. M. Shale gas potential of the lower Jurassic Gordondale member, northeastern British Columbia, Canada. *Bull. Can. Pet. Geol.* **2007**, *55*, 51–75.
- (16) Tian, H.; Li, T.; Zhang, T.; Xiao, X. M. Characterization of methane adsorption on over mature Lower Silurian Upper

Ordovician shales in Sichuan Basin, southwest China: Experimental results and geological implications. *Int. J. Coal Geol.* **2016**, *156*, 36–49.

- (17) Wang, S.; Song, Ž.; Cao, T.; Song, X. The methane sorption capacity of Paleozoic shales from the Sichuan Basin, China. *Mar. Pet. Geol.* **2013**, *44*, 112–119.
- (18) Zhang, T.; Ellis, G. S.; Ruppel, S. C.; Milliken, K.; Yang, R. Effect of organic matter type and thermal maturity on methane adsorption in shale-gas systems. *Org. Geochem.* **2012**, *47*, 120–131.
- (19) Weniger, P.; Kalkreuth, W.; Busch, A.; Krooss, B. M. Highpressure methane and carbon dioxide sorption on coal and shale samples from the Parana Basin, Brazil. *Int. J. Coal Geol.* **2010**, *84*, 190–205.
- (20) Gasparik, M.; Gensterblum, Y.; Ghanizadeh, A.; Weniger, P.; Krooss, B. M. High pressure/High temperature Methane-Sorption Measurements on Carbonaceus Shales by the Manometric Method: Experimental and Data-Evaluation Considerations for Improved Accuracy. SPE J. 2015, 20, 790–809.
- (21) Ji, W.; Song, Y.; Jiang, Z.; Wang, X.; Bai, Y.; Xing, J. Geological controls and estimation algorithms of lacustrine shale gas adsorption capacity: A case study of the Triassic strata in the southeastern Ordos Basin, China. *Int. J. Coal Geol.* **2014**, *134*–135, 61–73.
- (22) Cui, X.; Bustin, A. M. M.; Bustin, R. Measurements of gas permeability and diffusivity of tight reservoir rocks: Different approaches and their applications. *Geofluids* **2009**, *9*, 208–223.
- (23) Lu, X. C.; Li, F. C.; Watson, A. T. Adsorption measurements in Devonian shales. *Fuel* **1995**, *74*, 599–603.
- (24) Santos, J. M.; Akkutlu, I. Y. Laboratory Measurements of Sorption Isotherm Under Confining Stress With Pore-Volume Effects. *SPE Journal* **2013**, *18* (5), 924–931.
- (25) Sigal, R. F.; Akkutlu, I. Y.; Kang, S. M.; Diaz-Campos, M.; Ambrosse, R. J. The Laboratory Measurement of Gas Storage Capacity of Organic Shales. *Petrophysics* **2013**, *54*, 224–235.
- (26) Kang, S. M.; Shinn, Y. J.; Akkutlu, I. Y. Gas Storage Capacity of Iljik and Hasandong Shales in Gyongsang Basin, South Korea. *Proceedings of the Unconventional Resources Technology Conference*; Denver, CO, Aug 25–27, 2014; DOI: 10.15530/URTEC-2014-1922165.
- (27) Jarvie, D. M.; Hill, R. J.; Ruble, T. E.; Pollastro, R. M. Unconventional shale-gas systems: The Mississippian Barnett Shale of north-central Texas as one model for thermogenic shale-gas assessment. *AAPG Bull.* **2007**, *91*, 475–499.
- (28) Xiong, F.; Jiang, Z.; Li, P.; Wang, X.; Bi, H.; Li, Y.; Wang, Z.; Amooie, M. A.; Soltanian, M. R.; Moortgat, J. Pore structural of transitional shales in the Ordos Basin, NW China: Effects of composition on gas storage capacity. *Fuel* **2017**, *206*, 504–515.
- (29) Curtis, M. E.; Cardott, B. J.; Sondergeld, C. H.; Rai, C. S. Development of organic porosity in the Woodford Shale with increasing thermal maturity. *Int. J. Coal Geol.* **2012**, *103*, 26–31.
- (30) Ji, L. M.; Zhang, T.; Milliken, K. L.; Qu, J.; Zhang, X. Experimental investigation of main controls to methane adsorption in clay-rich rocks. *Appl. Geochem.* **2012**, *27*, 2533–2545.
- (31) Chalmers, G. R. L.; Bustin, R. M. The organic matter distribution and methane capacity of the Lower Cretaceous strata of Northeastern British Columbia, Canada. *Int. J. Coal Geol.* **2007**, 70, 223–239
- (32) Chalmers, G. R. L.; Bustin, R. M. Lower Cretaceous gas shales in northeastern British Columbia, Part I: Geological controls on methane sorption capacity. *Bull. Can. Pet. Geol.* **2008**, *56*, 1–21.
- (33) Kim, J.; Kim, D.; Lee, W.; Lee, Y.; Kim, H. Impact of total organic carbon and specific surface area on the adsorption capacity in Horn River shale. *J. Pet. Sci. Eng.* **2017**, *149*, 331–339.
- (34) Wang, Y.; Zhu, Y.; Liu, S.; Zhang, R. Pore characterization and its impact on methane adsorption capacity for organic-rich marine shales. *Fuel* **2016**, *181*, 227–237.
- (35) Xia, J.; Song, Z.; Wang, S.; Zeng, W. Preliminary study of pore structure and methane sorption capacity of the Lower Cambrian shales from the north Gui-Zhou Province. *J. Nat. Gas Sci. Eng.* **2017**, 38, 81–93.

(36) Mendhe, V. A.; Mishra, S.; Varma, A. K.; Kamble, A. D.; Bannerjee, M.; Sutay, T. Gas reservoir characteristics of the Lower Gondwana Shales in Raniganj Basin of Eastern India. *J. Pet. Sci. Eng.* **2017**, *149*, 649–664.

- (37) Zhang, Y.; Shao, D.; Yan, J.; Jia, X.; Li, Y.; Yu, P.; Zhang, T. The pore size distribution and its relationship with shale gas capacity in organic-rich mudstone of Wufeng-Longmaxi Formations, Sichuan Basin, China. *J. Nat. Gas Geosci.* **2016**, *1*, 213–220.
- (38) Chen, L.; Jiang, Z.; Liu, K.; Ji, W.; Wang, P.; Gao, F.; Hu, T. Application of Langmuir and Dubinin-Radushkevich models to estimate methane sorption capacity on two shale samples from the Upper Triassic Chang 7 Member in the southeastern Ordos Basin, China. *Energy Explor. Exploit.* **2017**, *35*, 122–144.
- (39) Gensterblum, Y.; Busch, A.; Krooss, B. M. Molecular concept and experimental evidence of competitive adsorption of H₂O, CO₂ and CH₄ on organic material. *Fuel* **2014**, *115*, 581–588.
- (40) Barrero, D.; Pardo, A.; Vargas, C.; Martínez, J. Colombian Sedimentary Basins: Nomenclature, Boundaries and Petroleum Geology, a New Proposal; Agencia Nacional de Hidrocarburos (ANH): Bogotá, Colombia, 2007; pp 92.
- (41) Chung, F. H. Quantitative interpretation of X-ray diffraction patterns of mixtures. II. Adiabatic principle of X-ray diffraction analysis of mixtures. *J. Appl. Crystallogr.* **1974**, *7*, 526–531.
- (42) Brunauer, S.; Emmett, P. H.; Teller, E. Adsorption of gases in multimolecular layers. *J. Am. Chem. Soc.* **1938**, *60*, 309–319.
- (43) Heller, R.; Vermylen, J.; Zoback, M. Experimental investigation of matrix permeability of gas shales. *AAPG Bull.* **2014**, *98*, 975–995.
- (44) Pino, D.; Bessieres, D. CH₄/CO₂ Mixture Adsorption on a Characterized Activated Carbon. *J. Chem. Eng. Data* **2017**, *62*, 1475–1480
- (45) Wagner, W.; Span, R. Special Equations of State for Methane, Argon and Nitrogen for the temperature range from 270 to 350K at pressures up to 30 MPa. *Int. J. Thermophys.* **1993**, *14* (4), 699–725.
- (46) Hou, Y. G.; He, S.; Yi, J. Z.; Zhang, B.; Chen, X.; Wang, Y.; Zhang, J.; Cheng, C. Y. Effect of pore structure on methane sorption capacity of shales. *Pet Explor Dev.* **2014**, *41*, 272–281.
- (47) Chareonsuppanimit, P.; Mohammad, S. A.; Robinson, R. L., Jr.; Gasem, K. A. M. High- pressure adsorption of gases on shales: Measurements and modeling. *Int. J. Coal Geol.* **2012**, *95*, 34–46.
- (48) Rexer, T. F. T.; Benham, M. J.; Aplin, A. C.; Thomas, K. M. Methane adsorption on shale under simulated geological temperature and pressure conditions. *Energy Fuels* **2013**, *27*, 3099–3109.
- (49) Dreisbach, F.; Staudt, R.; Keller, J. U. High Pressure Adsorption Data of Methane, Nitrogen, Carbon Dioxide and their Binary and Ternary Mixtures on Activated Carbon. *Adsorption* **1999**, *5*, 215–227.
- (50) Yang, F.; Ning, Z. F.; Liu, H. Q. Fractal characteristics of shales from a shale gas reservoir in the Sichuan Basin, China. *Fuel* **2014**, *115*, 378–384.
- (51) Gensterblum, Y.; VanHemert, P.; Billemont, G.; Busch, A.; Charriere, D.; Li, D.; Krooss, B. M.; deWeireld, G. D.; Prinz, K.; Wolf, H. A. A. European inter-laboratory comparison of high pressure CO₂ sorption isotherms. I: Activated Carbon. *Carbon* **2009**, *47*, 2958–2969.
- (52) Yuan, W.; Pan, Z.; Li, X.; Yang, Y.; Zhao, C.; Connell, L. D.; Li, S.; He, J. Experimental study and modelling of methane adsorption and diffusion in shale. *Fuel* **2014**, *117*, 509–519.
- (53) Pozo, M.; Pino, D.; Bessieres, D. Effect of thermal events on maturation and methane adsorption of ammonium Illite-rich Silurian black shales (Checa, Spain). *Appl. Clay Sci.* **2017**, *136*, 208–218.
- (54) McCarthy, K.; Rojas, K.; Niemann, M.; Palmowski, D.; Peters, K.; Stankiewicz, A. Basic Petroleum Geochemistry for Source Rock Evaluation. *Oilfield Rev.* **2011**, *23*, 32–43.
- (55) Peters, K. E. Guidelines for evaluating petroleum source rock using programmed pyrolysis. AAPG Bull. 1986, 70, 328–329.
- (56) Gorin, G. E.; Feist-Burkhardt, S. Organic facies of Lower to Middle Jurassic sediments in the Jura Mountains, Swizerland. *Rev. Palaeobot. Palynol.* **1990**, 65, 349–355.
- (57) Xu, J.; Bechtel, A.; Sachsenhofer, R. F.; Liu, Z.; Gratzer, R.; Meng, Q.; Song, Y. High resolution geochemical analysis of organic

matter accumulation in the Qingshankou Formation, Upper Cretaceous, Songliao Basin (NE China). *Int. J. Coal Geol.* **2015**, *141–142*, 23–32.

- (58) Cao, T.; Song, Z.; Wang, S.; Xia, J. A comparative study of the specific surface area and pore structure of different shales and their kerognes. *Sci. China: Earth Sci.* **2015**, *58*, 510–522.
- (59) Gasparik, M.; Rexer, T. F. T.; Aplin, A. C.; Billemont, P.; De Weireld, G.; Gensterblum, Y.; Henry, M.; Krooss, B. M.; Liu, S.; Ma, X.; Sakurovs, R.; Song, Z.; Staib, G.; Thomas, K. M.; Wang, S.; Zhang, T. First international inter-laboratory comparison of high-pressure CH₄, CO₂ and C₂H₆ sorption isotherms on carbonaceus shales. *Int. J. Coal Geol.* **2014**, *132*, 131–146.
- (60) Li, P.; Jiang, Z.; Zheng, M.; Bi, H.; Chen, L. Estimation of shale gas adsorption capacity of the Longmaxi Formation in the Upper Yangtze Platform, China. *J. Nat. Gas Sci. Eng.* **2016**, *34*, 1034–1043.
- (61) Murillo, C.; Gomez, O.; Ortiz Cancino, O.; Muñoz, S. Aplicación de modelos para la generación de la isoterma de adsorción de metano en una muestra de shale y su impacto en el cálculo de reservas. *Revista Fuentes* **2015**, *13* (2), 131–140.